Influence of Different Sterilization Procedures on the Morphological Parameters and Mechanical Properties of Ultra-High-Molecular-Weight Polyethylene*

V.-M. Archodoulaki, T. Koch, A. Rodriguez, S. Seidler

Institute of Materials Science and Technology, Vienna University of Technology, Favoritenstrasse 9-11, 1040 Vienna, Austria

ABSTRACT: The objectives of this study were to examine the effects of the processing conditions, sterilization, and thermal treatment on the morphological and mechanical properties of ultra-high-molecular-weight polyethylene (UHMWPE) in medical applications by means of thermal analysis, Fourier transform infrared spectroscopy, and nanoindentation. It is well known that manufacturing, irradiation, and thermal treatments significantly alter the microstructure of materials, which results in changes in their mechanical properties. UHMWPE was found to be barely sensitive to processing conditions but strongly influenced by sterilization treatments. Great emphasis was given to the characterization of the so-called first generation of highly crosslinked UHMWPE because the thermal history of this material differed from that of γ-irradiated materials. The physical and mechanical properties of UHMWPE were influenced as a result of γ and electron-beam irradiation and the remelting procedure. Lower crystallinity, different lamellar thickness distributions, and lower hardness and modulus values were estimated. © 2010 Wiley Periodicals, Inc. J Appl Polym Sci 120: 1875–1884, 2011

Key words: biomaterials; mechanical properties; morphology; polyethylene (PE)

INTRODUCTION

Many applications in different areas, such as mining, foundries, and transportation, have been found for ultra-high-molecular-weight polyethylene (UHMWPE). Moreover, UHMWPE is used in medicine for the manufacturing of artificial joints in most orthopedic implants, especially in hips and knees. Over the past 40 years, because it was introduced as a replacement for polytetrafluoroethylene in 1962, its biocompatibility, low coefficient of friction, and high wear resistance have made it a highly successful bearing material in these applications. Each year, about 1.4 million joint replacement procedures are performed around the world. Despite the success of these restorative procedures, implants containing UHMWPE have only a finite lifetime. Wear and damage of the UHMWPE components is one of the factors limiting implant durability. To produce medical-grade UHMWPE implants, the material has to be subjected to sterilization, irradiation, or other processing steps. In the irradiation step, γ and electron-beam (E-beam)

radiation produce free radicals in the UHMWPE. Regardless of whether the irradiation is conducted in air or in an inert environment, some of the free radicals will remain entrapped within the crystalline phase of the UHMWPE. If irradiation is done in air, these free radicals react with available oxygen and cause further time-dependent chemical degradation. The so-called first generation of highly crosslinked UHMWPE showed a lower wear rate than conventional UHMWPE.[1] Crosslinked materials undergo during the manufacturing process a postradiation melting or annealing process to reduce the concentration of free radicals and potential oxidative degradation.[2]

Crosslinked UHMWPE differs in the mechanical properties and *in vivo* performance from conventionally sterilized materials because the thermal and irradiation histories of this material differs from those of γ-irradiated materials.

In principle, there exist two common methods for crosslinking high-molecular-weight polyethylene: chemical crosslinking via peroxides and silanes, which is not used for artificial hip joints, and γ irradiation, or E beam. γ irradiation, or E beam, is a common method for the sterilization of implants since the 1960s. Nowadays, sterilization and crosslinking differ because of the used irradiation dose. Although sterilization is commonly performed at about 25 kGy, crosslinking is done by the exposure

of materials to a dose of 75–100 kGy. The wear rate depends on the irradiation dose; up to a dose of 100 kGy, there is an important reduction in the wear rate.[3]

A versatile test method for determining the structure parameters on a nanometer scale is differential scanning calorimetry (DSC). It can be used for the determination of the degree of crystallinity (X_c) and allows for the calculation of lamellar thickness (L_C) and L_C distribution of semicrystalline polymers.[4–6] The determination of the density of UHMWPE also gives information about the morphology, as the density of the crystalline phase is higher then that of the amorphous phase. Because of the reduced crystallinity by the crosslinking of the material, the density is also reduced.[7,8]

In this study, DSC investigations and calculations of the L_C and L_C distribution were conducted. Because the crystallinity and crystal orientation have a strong impact on the mechanical properties of the materials, investigations into the hardness (H_{IT}) and modulus of elasticity in terms of nanoindentation were performed. Fourier transform infrared (FTIR) microscopy investigations allowed us to correlate the calculated oxidation index (OI; as a reference of oxidative degradation) to the calculated crystallinity from DSC and the determined mechanical properties.

EXPERIMENTAL

Materials

Four different samples were studied. Sample 1 was the raw material in powder form of a GUR 1020 without stearate (sample name: powder). The second sample was the same material, GUR 1020, but was ram-extruded in bar shape and unsterilized (sample name: unsterilized). The third sample was a ram-extruded bar of the same GUR 1020, sterilized with 25 kGy γ irradiation in N_2 (sample name: γ-sterilized). The fourth sample was a new hip implant, Durasul®, sterilized with ethylene oxide but previously crosslinked with a 95 kGy E-beam warm irradiation (at 125°C) and later remelted at 150°C for 2 h (sample name: crosslinked). Durasul® acetabular liners are manufactured from GUR 1050 compression-molded stock. A good overview of the manufacturing process of Durasul® is given in ref. 2. GUR 1020 and GUR 1050 were reported with average molecular weights of 3.5×10^6 and 5.5 to 6×10^6 g/mol, respectively. An overview of the average properties for GUR 1020 and 1050 grades is given in ref. 9. Fischer[10] reported for crosslinked GUR 1050 compared to conventional noncrosslinked GUR 1020 a fourfold less wear volume (9 mm³/mc); this was only two times lower that the osteolytic potential.

To distinguish these samples from samples cooled at a defined cooling rate for further nanoindentation experiments, this group was called the *processed state*.

Methods

X_c, the melting temperature (T_m), and the calculation of L_C were conducted by experiments with DSC. As reported in ref. 11, X_c of UHMWPE varies between 39 and 75% and its T_m varies between 125 and 138°C.

The DSC experiments were performed with a DSC 2920 instrument (TA Instruments, New Castle, DE), with nitrogen as a purge gas at a flow rate of 50 mL/min, heating and cooling rates of 10 K/min, and sample masses of about 5 mg. A typical procedure was as follows: the sample was heated from ambient temperature to 160°C and held at this temperature for 5 min. Then, it was followed by cooling to ambient temperature at a cooling rate of 10 K/min. After it was held at this temperature for 5 min, the sample was reheated to 160°C at 10 K/min.

UHMWPE is a linear semicrystalline polymer, which can be described as a two-phase composite. One phase is the crystalline phase, in which chains can fold and orient themselves into highly ordered lamellae with the crystals being orthorhombic in structure. According to ref. 12, the crystalline lamellae range in thickness from 10 to 50 nm. In virgin UHMWPE, the lamellae are randomly oriented in the amorphous phase of the polymer. The crystallinity (X) was calculated with a heat of fusion (ΔH_f) of pure UHMWPE of 288 J/g[11] and the following expression:

$$X(\%) = \frac{\Delta H_{\text{endotherm}}}{\Delta H_f} \qquad (1)$$

where the enthalpy ($\Delta H_{\text{endotherm}}$) was calculated by the integration of the endothermic peak. All integrations were calculated between 80 and 155°C for the first (processed state) and second heatings to compare the different samples.

There are two different ways to calculate the probability of L_C distribution curves. The first method is to use DSC endotherms directly; specifically, the melting endotherms are assumed to be proportional to the mass fraction of crystalline lamellae that melt at a specific temperature. The second method is to use a differential equation, developed by Alberola et al.,[4] based on the mathematical equality of mass fraction of the crystalline phase to the ratio of the normalized heat of melting to the enthalpy of fusion.[13]

It is known that the temperature affects the crystallization kinetics, and on the other hand, the

lamella thickness affects T_m of the polymer crystals. Structural regular polymers normally solidify into lamellar crystals, the T_m of which is inversely related to L_C. This relationship is expressed in the form of the Gibbs–Thomson equation:[5,6,14]

$$T_m = T_m^0 \left(1 - \frac{2\sigma_e}{\Delta H_f L_c}\right) \tag{2a}$$

where T_m is the observed melting temperature for a crystalline lamella of thickness L_C, T_m^0 is the equilibrium melting temperature of the crystalline lamella of infinite thickness, σ_e is the free surface energy of the basal surface of the crystalline lamella and is associated with the energy of chain folding during the crystallization process, and ΔH_f is the enthalpy of fusion for the crystalline phase.

The values of these parameters are the following: $\sigma_e = 9.3 \times 10^{-2}$ J/m^2 (surface free energy), $\Delta H_f = 2.80 \times 10^8$ J/m^3 (ΔH_f for the crystalline phase), and $T_m^0 = 418.95$ K (T_m of a crystal of infinite thickness).[12,15–17]

L_C was estimated with the T_m collected from the DSC experiments and by means of the following formula:

$$L_c = \frac{2\sigma_e}{\Delta H_f} \left(1 - \frac{T_m}{T_m^0}\right)^{-1} \tag{2b}$$

This formula shows that the T_m of a semicrystalline material can be related to the average thickness of the crystallites within it.

A more complex situation exists for polymers that have nonequilibrium distributions of crystal thickness (e.g., copolymers) and for polymers that show a melting behavior that extends over a large temperature range and certainly involves the fusion of crystals with different thicknesses. For that reason, the DSC melting endotherms can be used to calculate the L_C distribution. In this approach, a DSC profile, heat flow versus temperature, is transformed into an L_C distribution curve (probability of the mass percentage of lamellae vs L_C) with the Gibbs–Thomson equation [eq. (2)].[16] The thickness distribution of the crystalline lamellae, related to the DSC, may be expressed by the following equation:

$$f(L) = \frac{1}{M}\frac{dM}{dL} \tag{3}$$

where M is the mass of crystalline phase within the sample for the DSC experiment and dM is the fraction of the crystalline phase with a thickness in the range $L+dL$.

The method uses a differential equation based on the mathematical equality of the mass fraction of the crystalline phase to the ratio of the normalized heat of melting to the enthalpy of fusion, which leads to

the following formula. Using the Gibbs–Thomson equation, Alberola and coworkers[4–6] developed a model to express the L_C distribution from DSC endotherms as follows:

$$\frac{1}{M}\frac{dM}{dL} = \frac{dE}{dT}\frac{(T_m^0 - T_m)^2 \rho_c}{2\sigma_e T_m^0 M} \tag{4}$$

where dM is the mass of the crystalline phase, which has a L_C between L and $L + dL$ and melts between the temperature (T) and $T + dT$; dE/dT, measured by the DSC endotherms, is the energy required to melt the dM fraction of the crystalline phase; and ρ_c is the density of the crystal phase. The L_C distribution is obtained by the plotting of $1/M\ dM/dL$ versus L.[6] At this point, it is important to emphasize that ρ_c for UHMWPE is 1.005 g/cm^3.[6] All the other parameters in the above equation have the same definitions as in equation 2a.

The evaluation of the following equation was based on the DSC measurements:[4]

$$\frac{dE}{dT}\frac{1}{M}\left(\frac{J}{{}^\circ C}\frac{1}{kg}\right) = \frac{\text{Heat flow}\left(\frac{J}{kg\ min}\right)}{\text{Heating rate}\left(\frac{{}^\circ C}{min}\right)} \tag{5}$$

The heat flow is the value of the ordinate on the original DSC curve, and it can be used in eq. (4) as follows:

$$\begin{aligned}\frac{1}{M}\frac{dM}{dL} &= \frac{dE}{dTM}\frac{(T_m^0 - T_m)^2 \rho_c}{2\sigma_e T_m^0} \\ &= \frac{\text{Heat flow}}{\text{Heating rate}}\frac{(T_m^0 - T_m)^2 \rho_c}{2\sigma_e T_m^0}\end{aligned} \tag{6}$$

The values used for the calculation were $T_m^0 = 418.7$ K, $\rho_c = 1.005$ g/cm^3, $\Delta H_f = 2.80 \times 10^8$ J/m^3 = 288 J/g, and $\sigma_e = 9.3 \times 10^{-2}$ J/m^2.[5]

The density measurement is based on the Archimedean principle. The mass fraction crystallinity is given by

$$X_c = \frac{\rho_c}{\rho}\left(\frac{\rho - \rho_a}{\rho_c - \rho_a}\right) \tag{7}$$

where ρ, ρ_c, and ρ_a are the densities of the sample, the crystalline phase, and the amorphous phase, respectively. ρ_c was 1.005, and ρ_a was 0.85 g/cm^3.

FTIR spectroscopy was carried out with an FTIR spectrometer (Tensor 27, Brucker Optics, Germany). The line-scan spectra were based on 32 scans and a resolution of 4 cm^{-1}. The scanned wave-number range was from 4000 to 600 cm^{-1}. The measurements were performed in transmittance modus in samples cut to a 20-μm thickness with a microtome; a metal knife was used because less interference occurred.

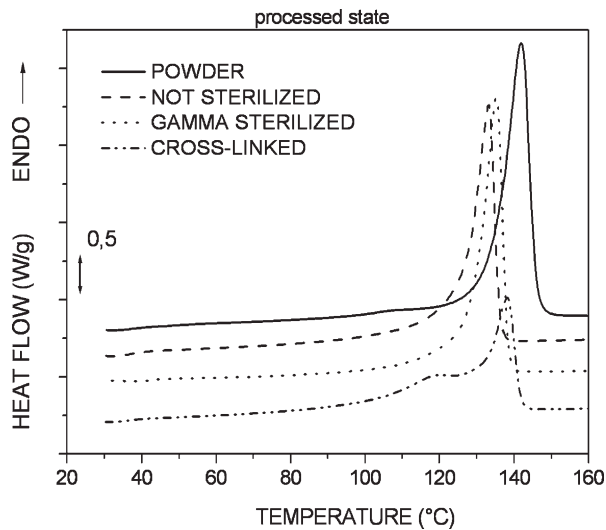**Figure 1** DSC curves of the processed state (first heating run).

The carbonyl peak was quantified in every spectrum based on ISO 5834-4 : 2005,[18] which describe the technique to determine the OI. The carbonyl peak was defined as the ratio of the area of the absorption peak between 1650 and 1850 cm^{-1} [oxidation peak area (OA)] to the area of the absorption peak between 1330 and 1396 cm^{-1} [normalization peak area (ON)], as given in eq. (8):

$$OI = \frac{OA}{ON} = \frac{A_{1650 \text{ to } 1850 \text{ cm}^{-1}}}{A_{1330 \text{ to } 1396 \text{ cm}^{-1}}}$$ (8)

Instrumented indentation testing is a powerful set of tools for the investigation of the mechanical properties of materials in small dimensions. In such a test, a hard tip, typically a diamond, is pressed into the sample with a known load. After some time, the load is removed. H_{IT} can be calculated with the following equation:

$$H_{IT} = \frac{P}{A} = \frac{P}{24.5h_c^2}$$ (9)

where P is the load applied to the test surface and A and h_c are the projected contact area and contact depth, respectively, at that load.

The elastic modulus (E) of the test sample is determined from the reduced modulus (E_r) given by[19]

$$E_r = \frac{\sqrt{\pi} S}{2\beta\sqrt{A}}$$ (10)

where β is a constant that depends only on the geometry of the indenter, S is the unload stiffness, A is the area, and P is the load applied to the test surface.

The indentation modulus (E_{IT}) of the test material is calculated with the expression[19]

$$\frac{1}{E_r} = \frac{(1 - v^2)}{E_{IT}} + \frac{(1 - v_i^2)}{E_i}$$ (11)

where v is the Poisson's ratio for the test material (in the case of UHMWPE, it is 0.43[20]) and E_i and v_i are the elastic modulus and Poisson's ratio, respectively, of the indenter. For diamond, these constants were $E_i = 1141$ GPa and $v_i = 0.07$.

For the indentation measurements, the specimens were embedded in an Araldite resin, water-cooled grinded, and polished by application of only a very low pressure. Indentation measurements with a Nano Indenter XP (Nano Instruments, Inc., Oak Ridge, TN) were carried out with depth controlled at a rate of 250 nm/s up to a maximum depth of 5 μm; samples were then held at maximum load for 30 s followed by unloading. A holding time of 30 s minimized the effect of creep on the unloading curve.

RESULTS

The results of the DSC measurements, a comparison of the first and second heating runs, are shown in Figures 1 and 2.

For the first heating run, representing the processed state (Fig. 1), the unsterilized and γ-sterilized samples showed the same T_m around 135°C, but the powder sample showed a higher T_m around 141°C. In the second heating run (Fig. 2), the unsterilized and γ-sterilized samples and the powder showed similar T_m's.

T_m of the powder sample at the first heating run was higher than that in the processed material. This elevated temperature was associated with the
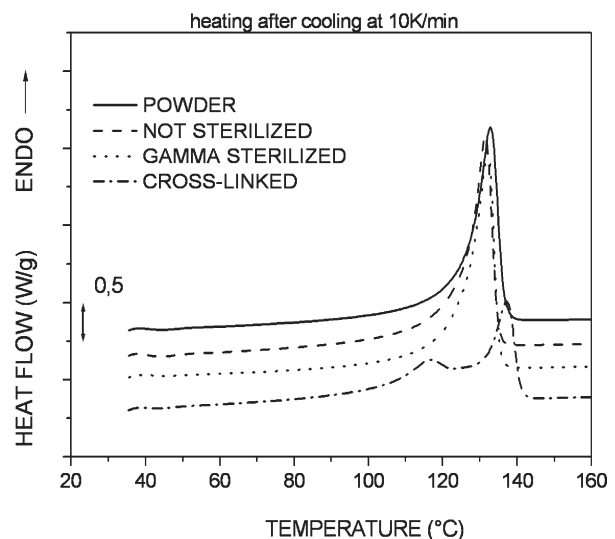

Figure 2 DSC curves after controlled cooling (second heating run).

crystalline morphology possessing considerable strain arising through crystallization in a shear field created because of the temperature gradient at the polymerization.[17]

In both heating runs, the crosslinked sample showed a double peak with maxima located at 118 and 138°C. These maxima indicated a heterogeneous, two-phase melting behavior. The double peak of the crosslinked sample in both heating runs could not be explained in terms of annealing effects because it was detectable in both heating runs and also in the cooling section. The latter one is typical for a fractionated crystallization. Presumably, the material shows a bimodal L_C distribution.

According to Medel et al.,[21] remelting and annealing treatments create a decrease in L_C, although the remelting process provides a stronger slimming of lamellae than the annealing step. TEM micrographs, as reported by Muratoglu et al.[22] and Medel et al.,[21] showed a bimodal distribution of L_C, which explained the two melting peaks observed in the DSC thermogram.

As denoted before, the material was radiated with E beam and then sterilized with epoxyethane (ethylene oxide). With this treatment and according to the literature,[23,24] a crosslinking process was generated with two kind of crosslinks: Y crosslinks and H crosslinks. The Y crosslink could be interpreted as a branching in two dimensions. The appearance of the double peak in both heating runs but also in the cooling section of the DSC experiments (Fig. 3) was evidence of crosslinking.

By integration of the endothermic peaks, the melting enthalpy of the crystalline phase was calculated. The calculations of the crystallinity according to eq. (1) and with $\Delta H_f = 288$ J/g[11] for all of the materials are shown in Table I.

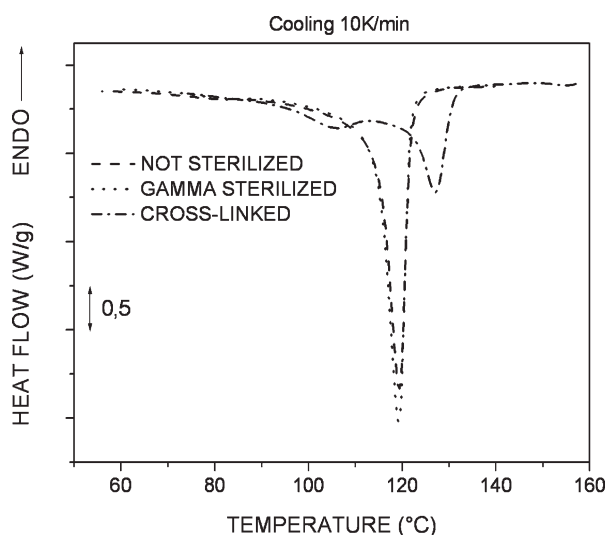**Figure 3** Crystallization behavior of the samples.

TABLE I
X_c and L_C Values for All of the Samples

Sample	Crystallinity (%)		L_C (nm)	
	First run	Second run	First run	Second run
Powder	70.8	51.8	68.9 ± 1.1	21.5 ± 0.2
Unsterilized	54.0	52.9	22.0 ± 0.3	19.7 ± 0.0
γ-sterilized	61.9	57.8	27.1 ± 0.5	20.5 ± 0.1
Crosslinked	51	47.4	10.4 ± 0.01	9.1 ± 0.01
			36.5 ± 0.7	33.2 ± 0.06

The measured density reflected the crystallinity because the density was composed *pro rata* from the higher density of the crystalline phase and the lower density of the amorphous phase.

In Table II, the determined density and the calculated crystallinity [according to eq. (7)] of the samples are shown. The crystallinity determined by DSC was slightly lower than the crystallinity calculated from the density. This might have been due to the interfacial phase between the crystalline and amorphous phases, which had an effect on the density and was not considered by the calculations of the melting enthalpy.

According to these results, the crystallinity and density of the γ-sterilized sample were slightly higher than those of the unsterilized sample. This could be an indication of chain scission. When a material is sterilized by γ irradiation in an inert gas, the main process is crosslinking, but it is also possible that chain scissions occur even in the presence of a very small amount of oxygen. Chain scission produces shorter molecules that lead to a higher crystallinity and a slightly higher density in materials. Comparing the DSC results of the cooling section for the unsterilized and γ-sterilized samples, we found a higher crystallization enthalpy for the γ-sterilized sample (Fig. 3). According to the results presented in Tables I and II, the crosslinked sample had the lowest crystallinity and density.

Not only the melting enthalpy and the crystallinity can be calculated from the DSC endotherms; also, information about the L_C and L_C distribution can be gleaned.

The mean L_C was calculated according to eq. (4b); in Table I, these values are compared. Although for the powder sample, L_C was higher in the first heating run, the γ-sterilized sample showed a higher L_C

TABLE II
Results of the Density Measurements

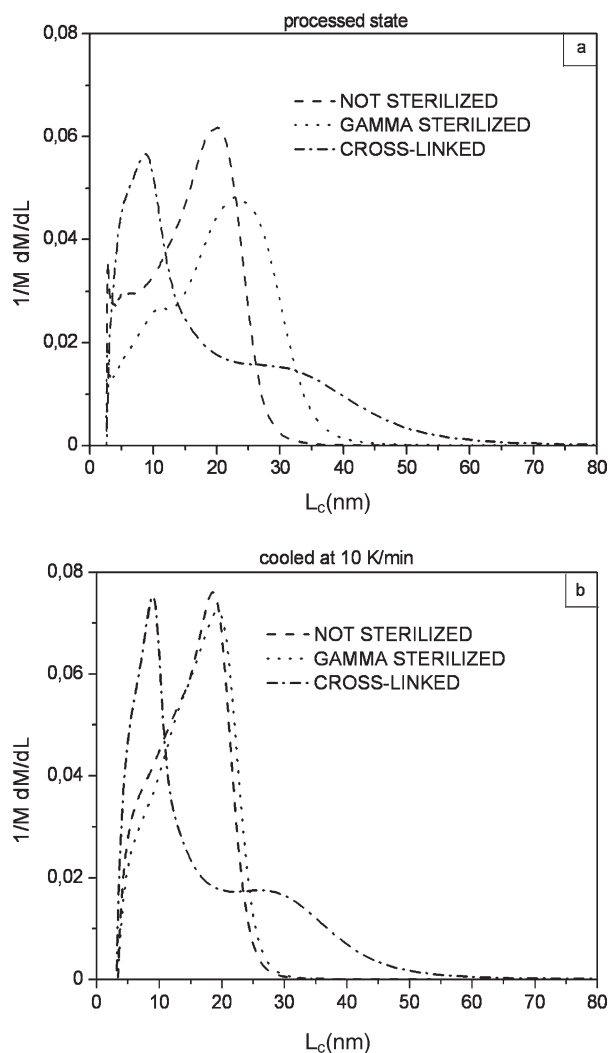| Sample	Density (g/cm³)	Crystallinity (%)
Unsterilized	0.9343	58.5
γ-sterilized	0.9451	65.2
Crosslinked	0.926	53.2

Figure 4 L_C distributions of the samples (a) in the processed state and (b) after controlled cooling at 10 K/min.

than the unsterilized sample. After the controlled cooling section, the L_C values for the three samples were almost comparable (Table I). For the crosslinked sample, no single L_C, according to eq. (4b), could be calculated because the DSC curve showed two maxima. This fact reflects the general problem of such simple calculations. For that reason, the L_C distributions for the unsterilized, γ-sterilized, and crosslinked samples were calculated according to eq. (6); a comparison of the calculated results is given in Figure 4(a) for the first heating run. The L_C distribution for the crosslinked material (crosslinked sample) differed, as expected, from the L_C distribution of the other materials. With regard to the results in Figure 4(a), the crosslinked material showed a bimodal distribution with a higher amount thinner lamellae and a lower amount of thicker lamellae.

This form of distribution can be evidence of Y branching or H branching. After the irradiation step, the UHMWPE was reheated over the T_m at 150°C.

The crystallization was then, because of the crosslinks built through the cooling sequence, hindered; X_c was lower, and a higher amount of thinner lamellae was generated. After the cooling section with a controlled cooling velocity, the calculation of the L_C distributions for the unsterilized, γ-sterilized, and crosslinked samples [Fig. 4(b)] showed a bimodal distribution for the crosslinked material and similar distributions for the unsterilized and γ-sterilized samples.

The results of the FTIR investigations performed in transmittance mode are shown in Figure 5(a,b). The main peaks found in the spectrum of the UHMWPE are given in detail in refs. 17, 23, and 25–27. The most interesting peaks that were evident in all of the spectra of UHMWPE are denoted in Table III.

As shown in Figure 5(a), the carbonyl peak at 1720 cm^{-1} (ketone–aldehyde peak) underlines the most important difference between all of the samples. It is obvious that oxidation led to carbonyl
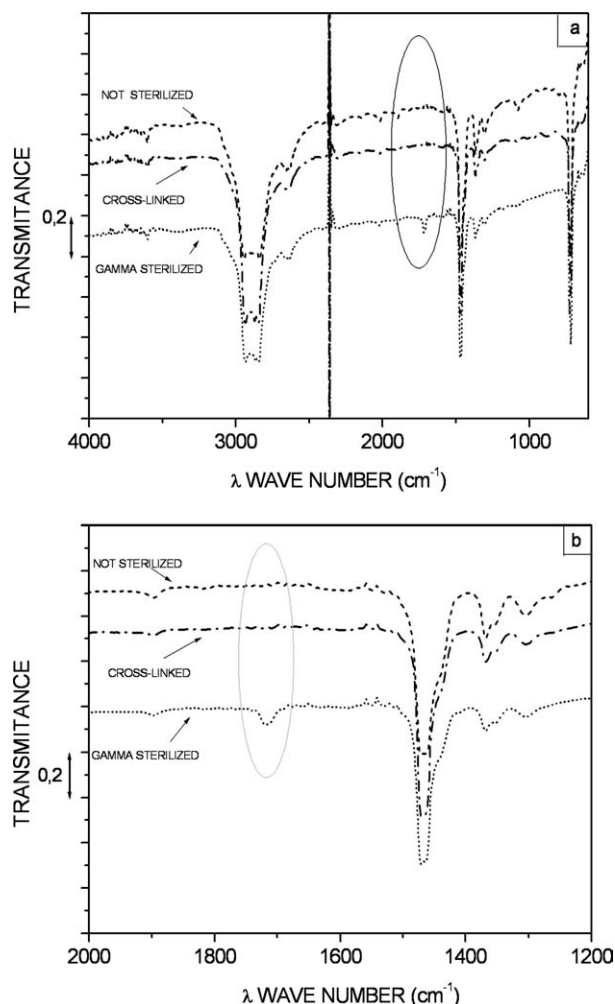

Figure 5 (a) FTIR investigations of the samples and (b) detail of the spectrum of the FTIR investigations: carbonyl peak.

TABLE III
Main IR Absorption Peaks of UHMWPE

	Name	Region (cm^{-1})
Polyethylene methylene (CH_2) vibration	Bending	1463–1473
	Rocking	720
	Twisting	2022
Ethylene region (CH_2—CH_2)		2915–2849
Carbonyl group		1689–1756
Methylene bending		1368
Vinyl group		990–909

group formation in the γ-sterilized sample. On the other hand, the unsterilized sample and the crosslinked sample did not show any peaks in this region [Fig. 5(b)].

To quantify the oxidation level of the samples, OI was calculated with the ISO/DIS 5834 technique [eq. (8)]. Typically, the oxidation levels calculated from UHMWPE implants immediately after γ sterilization in air exhibited an OI level above 0.1.[28] The results of these calculations are shown in Table IV. The calculated values of the unsterilized and crosslinked samples were hardly detectable and presented a lower OI level, whereas the γ-sterilized sample showed a higher OI level.

Manufacturing, irradiation, and thermal treatments significantly alter the microstructure. Changes in the crystallinity, distribution, and size of lamellae, tie molecules, and interfaces between amorphous and crystalline regions and the presence of new crystallites can be induced. This may result in changes in the structural and mechanical properties and also weakening of the properties of the materials. The influences of these changes on the mechanical properties of the materials are still unclear.[29,30]

There is a lack of knowledge concerning the mechanical properties (especially collected by the nanoindentation method) of Durasul®.

Furthermore, when already published data for different UHMWPE materials were compared, there were many differences in the reported values. Lewis[31] published a table for the modulus of elastic-

ity with the calculated mean of the means and standard deviation of the means for different uncrosslinked and crosslinked materials of 915 ± 423 and 860 ± 206 MPa, respectively. This fact implies that different sterilization and crosslinking procedures but also different applied measuring conditions lead to incomparable results.

As Medel et al.[21] discussed, thermal treatments such as remelting and annealing change the microstructure of material, and these changes are reflected in the mechanical properties. Published data of crosslinking products show different micromechanical properties because they differ in terms of remelting and annealing temperatures and irradiation procedures.

The results of the microhardness tests are shown in Figures 6 and 7. Because of the calculated lower crystallinity of the crosslinked product, one could suppose that the ductility and toughness increased. In both states, after processing and after defined cooling at a rate of 10°K/min, the crosslinked material showed the lowest H_{IT} and E_{IT} values, whereas the sterilized material showed the highest values (Fig. 6). As it was found in the literature[32] the procedure of crosslinking combined with further (thermal) treatment enhances the wear behavior but reduces other mechanical properties, including strength, ductility, fracture toughness, and crack propagation resistance.

In striking contrast to other reported values of microhardness,[33–35] Flores et al.[36] studied polyethylene implants before and after use by means of microhardness tests (using a Vickers diamond and a Leitz microindentation tester). The estimated values for the control sample (nonimplanted acetabular insert) showed a H_{IT} value of 57 MPa, which fit good with our results. As discussed already for the elastic modulus values, also big variations of the reported values for the microhardness were demonstrated when we took into account that, for example, Tretinnikov at al.[37] reported values for the microhardness of the unirradiated UHMWPE surface in the range of 0.35 GPa.

TABLE IV
Calculated OI Values

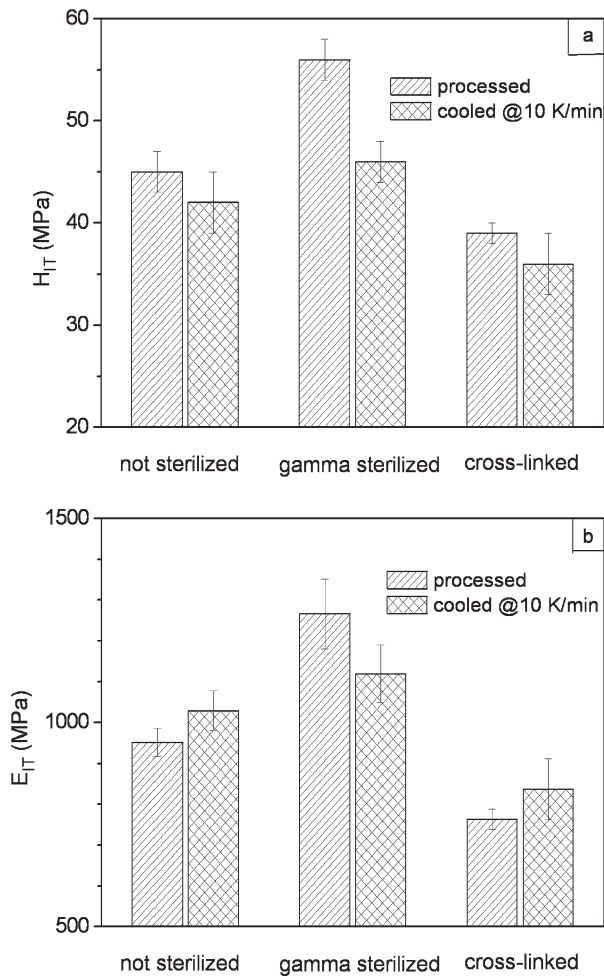| SAMPLE	OA	ON	OI	OI average	Deviation
Unsterilized					
Sample 1	0.139	3.432	0.040	0.043	0.0025
Sample 2	0.149	3.276	0.045		
Crosslinked					
Sample 1	0.298	2.239	0.133	0.108	0.0251
Sample 2	0.168	2.026	0.082		
γ-sterilized					
Sample 1	2.064	1.699	1.215	1.188	0.0271
Sample 2	1.927	1.660	1.161		

Figure 6 (a) H_{IT} and (b) E_{IT} of the investigated materials.

As shown in Figure 6, the estimated values for H_{IT} and E_{IT} in dependence on the condition (processed state and samples cooled at a defined cooling

rate) showed deviant behavior. For that reason, the ratios of the estimated values between the crosslinked material and the unsterilized material and between the γ-sterilized material and the unsterilized material were calculated.

The H_{IT} and the E_{IT} ratio values of the crosslinked material to the unsterilized material were comparable in the processed state and in the controlled cooled state, whereas the ratios between the γ-sterilized and the unsterilized material were much higher in the processed state than in the controlled cooled state (Table V). This fact could be evidence that, because of the sterilization procedure, obviously the development of the morphology was more sensitive.

There was good linear dependence of H_{IT} on X_c [Fig. 7(a)]. The often observed parallel behavior of the indentation of indentation hardness and indentation modulus was not found. There was no common correlation between the modulus and crystallinity; a splitting of the linear functions for the processed state and the controlled cooled samples took place [Fig. 7(b)]. The reason for that is unclear. This shows that E_{IT} is not only controlled by the crystallinity; the role of the thickness of the lamellae and the amorphous regions is not negligible. Principally, the shape of the indentation curves was comparable, so a distinct different deformation behavior could be excluded. One possible explanation could be that the controlled cooled samples, which are slightly softer than the processed ones, showed more pileup during loading; this influenced the first stages of the unloading process used for the determination of the modulus. This led to an overestimated E_{IT}. After unloading, the pileup in low-crystalline samples is often smaller because of the higher viscoelastic
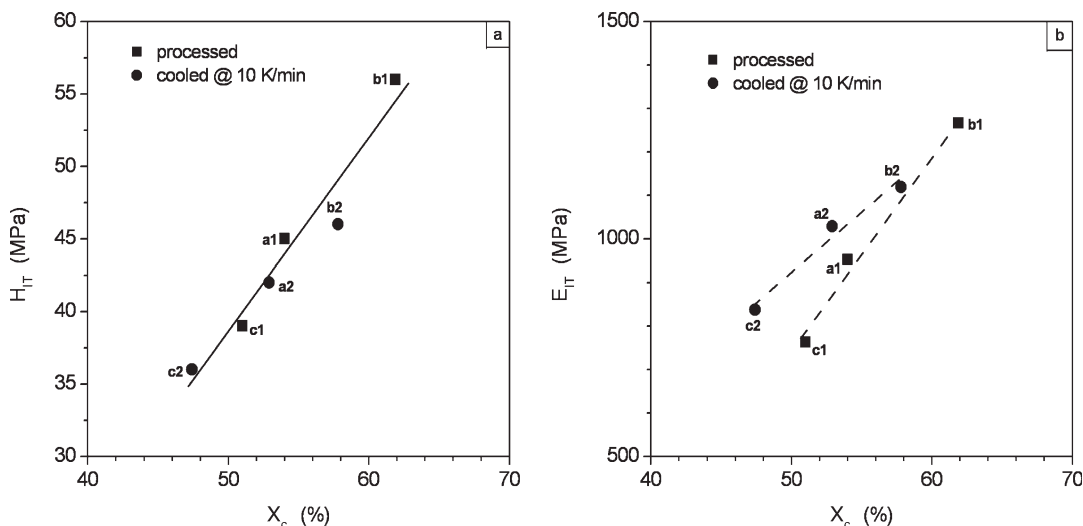

Figure 7 (a) H_{IT} and (b) E_{IT} dependence on the degree of crystallinity (X_c): (a1,a2) unsterilized, (b1,b2) γ-sterilized, and (c1,c2) crosslinked.

TABLE V
Ratios of the Indentation of H_{IT} to E_{IT} of the γ-Sterilized ($H_{IT,\gamma}$ and $E_{IT,\gamma}$) and the Crosslinked Samples ($H_{IT,x}$ and $E_{IT,x}$) to the Unsterilized Samples ($H_{IT,0}$ and $E_{IT,0}$)

	γ-sterilized		Crosslinked	
	$H_{IT,\gamma}/H_{IT,0}$	$E_{IT,\gamma}/E_{IT,0}$	$H_{IT,x}/H_{IT,0}$	$E_{IT,x}/E_{IT,0}$
Processed state	1.24	1.33	0.87	0.80
after dynamic crystallization at 10 K/min	1.10	1.09	0.86	0.81

recovery. Furthermore, in these softer samples, the amounts of viscoelastic deformation should have been higher than in the stiffer, higher crystalline processed samples. So, the deviation of the deformation behavior from the used elastic model was higher; this could also result in overestimated values of modulus. All these, partly opposite, effects, that is, crystallinity, thicknesses of the crystalline and amorphous regions, viscoelasticity and -plasticity, pileup, and the used model of calculation influenced the values of the determined modulus and could lead to correlations that are different from the correlation between H_{IT} and crystallinity.

Challenges for the correct measurement of the polymer mechanical properties in determining the modulus by indentation were reported in ref. 38.

The different elastic modulus values reported in this article compared with other reported values (e.g., Gilbert and coworkers[33,34] and Wernlé and Gilbert[35]) were explained by the mentioned facts (e.g., thermal treatments). In addition Maher et al.[39] reported that the elastic modulus of Durasul® (data collected by means of uniaxial tensile tests) was in the region of 800 MPa; this fit quite good with our results.

The results presented in this article followed principally the general rule that a higher crystallinity leads to a higher modulus. The correlation of E_{IT} and crystallinity ($R^2 = 0.84$) is quite good. The two linear correlations [depicted in Fig. 7(b)] depending on the processing were obvious, and the influence of the pressure during crystallization seems to be relevant. This is supported by the results in ref. 40. It was shown by Galeski[40] that for high-density polyethylene crystallized under different pressure conditions, there was no linear correlation between the modulus determined in compression testing and the crystallinity. He found that the elastic modulus was not solely controlled by X_c or by the crystal thickness or amorphous layer thickness. Crystallization under pressure caused differences in entanglement concentration, degree of chain span, and number of tie molecules.[40] These parameters can influence the response of a semicrystalline poly-

mer to strain in the elastic region and, therefore, the modulus.

To recapitulate the presented results, they were in agreement with the results discussed in ref. 25: the effects of irradiation on the mechanical properties are essentially a consequence of chain scission due to oxidation and of crosslinking. These, in turn, result in changes in the crystalline morphology (some rearrangement of molecules occurred), an increase in percentage crystallinity, a decrease in the effective entanglement density, and a decrease in the number of tie molecules. These result in changes in the tensile behavior, viscoelastic–plastic properties, fracture strength in different modes (including impact strength), fatigue strength, and wear.

CONCLUSIONS

Different UHMWPE materials were studied by DSC, FTIR microscopy, and nanoindentation. The DSC characterization revealed that some changes in the crystallinity occurred because of processing and thermal or mechanical deformation during manufacturing (ram extrusion).

X_c of the γ-sterilized sample was slightly higher than that of the unsterilized sample. The studied sample was sterilized in the absence of oxygen (in nitrogen) because of γ radiation. Radiation processes in the presence of oxygen (in air) induce chain scission, whereas radiation without oxygen lead to a partial crosslinking of UHMWPE. The crosslinking and chain scission reactions are not independent but influenced one another. They both take place competitively, and the chain scission, in general, accompanies the crosslinking reaction. Chain scissions leads to a decrease in the molar mass; shorter chains can fold easier, and because of that, the crystallinity and density of the material are higher.[41,42] The presumed chain scissions were confirmed by the FTIR measurements and the calculated higher OI of the γ-sterilized sample, which showed that, despite the nitrogen atmosphere, chain scissions occurred due to γ radiation.

When the crosslinked sample was compared with the γ-sterilized sample, different morphological parameters were apparent. X_c, the melting and crystallization behavior, and also L_C differed strongly because of the different thermal and sterilization histories. Also, a significantly lower density was detected.

Because different structures and morphologies showed different mechanical properties, the investigated material dependent structural parameters were correlated with the microhardness and modulus of elasticity.

The comparison of the chemical and mechanical properties showed that the γ-sterilized material with

the highest OI and higher crystallinity also showed the highest H_{IT} and modulus of elasticity. In the highly crosslinked material and the unsterilized material, OI was low; both showed a lower H_{IT} and modulus of elasticity. The lower H_{IT} of the crosslinked sample can be explained by the thermal after-treatment (remelting) reduced crystallinity and higher amount of thinner lamellae.

A linear dependence of H_{IT} on X_c was found.

For a better understanding of the effects of the sterilization and crosslinking procedures on the mechanical properties of UHMWPE, the ratios of H_{IT} and the E_{IT} of the crosslinked material and of the γ-sterilized material to the unsterilized material were calculated. The results show that, whereas for the crosslinked material the ratios were comparable in the processed state and in the controlled cooled state, the ratios of the γ-sterilized material were much higher in the processed state than in the controlled cooled state. Obviously, the development of morphology in the γ-sterilized material was more sensitive.

References

1. Affatato, S.; Bersaglia, G.; Rocchi, M.; Taddei, P.; Fagnano, C.; Toni, A. Biomaterials 2005, 26, 3259.
2. Jacobs, C. A.; Christensen, C. P.; Greenwald, A. S.; McKellop, H. J Bone Joint Surg Am 2007, 89, 2779.
3. Muratoglu, O. K.; Bragdon, C. R.; O'Connor, D. O.; Jasty, M.; Harris, W. H.; Gul, R.; McGarry, F. Biomaterials 1999, 20, 1463.
4. Alberola, N.; Cavaille, J. Y.; Perez, J. J Polym Sci Part B: Polym Phys 1990, 28, 569.
5. Romankievicz, A.; Sterzynski, T. Macromol Symp 2002, 180, 241.
6. Shen, F. W.; McKellop, H. A.; Salovey, H. J Biomed Mater Res A 1998, 41, 71.
7. Baker, D. A.; Hastings, R. S.; Pruitt, L. Polymer 2000, 41, 795.
8. Medel, F. J.; Garcia-Alvarez, F.; Gomez-Barrena, E.; Puertolas, J. A. Polym Degrad Stab 2005, 88, 435.
9. Muratoglu, O. K.; Kurtz, S. M. In Hip Replacement; Sinha, R. K., Ed.; Marcel Decker: New York, 2002.
10. Fisher, J.; Galvin, A.; Tipper, J.; Stewart, T.; Stone, M.; Ingham, E. In Bioceramics and Alternative Bearings in Joint Arthroplasty; D'Antonio, J. A.; Dietrich, M., Eds.; Steinkopff, 2005.
11. The UHMWPE Handbook: Ultra High Molecular Weight Polyethylene in Total Hip Joint Replacement; Kurtz, S. M., Ed.; Elsevier Academic: New York, 2004.
12. Sobieraj, M. C.; Kurtz, S. M.; Rimnac, C. M. Biomaterials 2005, 26, 6430.
13. Crist, B.; Mirabella, F. J Polym Sci Part B: Polym Phys 1999, 37, 3131.
14. Stephens, C. P.; Benson, R. S.; Martinez-Pardo, M. E.; Barker, E. D.; Walker, J. B.; Stephens, T. P. Nucl Inst Meth Phys Res B 2005, 236, 540.
15. Dos Santos, A. L.; Cassiano, L. F.; Miguez, J. C. Polym Test 2005, 24, 104.
16. Hongyi, Z.; Wilkes, G. L. Polym 1997, 38, 5735.
17. Cook, J. T. E.; Klein, P. G.; Ward, I. M.; Brain, A. A.; Farrar, D. F.; Rose, J. Polymer 2000, 41, 8615.
18. Implants for Surgery—Ultra-High-Molecular-Weight Polyethylene—Part 4: Oxidation Index Measurement Method; ISO 5834–4 : 2005.
19. Oliver, W. C.; Pharr, G. M. J Mater Res 1992, 7, 1564.
20. Park, K.; Mishra, S.; Lewis, G.; Losby, J.; Fan, Z.; Park, J. B. Biomaterials 2004, 25, 2427.
21. Medel, F. J.; Pena, P.; Cegonino, J.; Gomez-Barrena, E.; Puertolas, J. A. J Biomed Mater Res B 2007, 83, 380.
22. Muratoglu, O. K.; Bragdon, C. R.; O'Connor, D. O.; Jasty, M.; Harris, W. J Arthroplasty 2001, 16, 149.
23. Bracco, P.; Brunella, V.; Luda, M. P.; Zanetti, M.; Costa, L. Polymer 2005, 46, 10648.
24. Bracco, P.; Brach del Prever, E. M.; Cannas, M.; Luda, M. P.; Costa, L. Polym Degrad Stab 2006, 91, 2030.
25. Premnath, V.; Harris, W. H.; Jasty, M.; Merrill, E. W. Biomaterials 1996, 17, 1741.
26. Kurtz, S. M.; Muratoglu, O. K.; Buchanan, F.; Currier, B.; Gsell, R.; Greer, K.; Gualtieri, G.; Johnson, R.; Schaffner, S.; Sevo, K.; Spiegelberg, S.; Shen, F. W.; Yau, S. S. Biomaterials 2001, 22, 1731.
27. Premnath, V.; Bellare, A.; Merrill, E. W.; Jasty, M.; Harris, W. H. Polymer 1999, 40, 2215.
28. Muratoglu, O. K.; Harris, W. H. J Biomed Mater Res A 2001, 56, 584.
29. Puértolas, J. A.; Medel, F. J.; Cegonino, J.; Gomez-Barrena, E.; Ríos, R. J Biomed Mater Res B 2006, 76, 346.
30. Kurtz, S. M.; Villarraga, M. L.; Herr, M. P.; Bergstrom, J. S.; Rimnac, C. M.; Edidin, A. A. Biomaterials 2002, 23, 3681.
31. Lewis, G. Biomaterials 2001, 22, 371.
32. Kurtz, S. M.; Pruitt, L. A.; Jewett, C. W.; Foulds, J. R.; Edidin, A. A. Biomaterials 1999, 20, 1449.
33. Gilbert, J. L.; Cumber, J.; Butterfield, A. J Biomed Mater Res 2002, 61, 270.
34. Gilbert, J. L.; Merkhan, I. J Biomed Mater Res A 2004, 71, 549.
35. Wernleé, J. D.; Gilbert, J. L. J Biomed Mater Res B 2005, 75, 113.
36. Flores, A.; Jordan, N. D.; Balta-Calleja, F. J.; Bassett, D. C.; Olley, R. H.; Smith, N. G. Polymer 2000, 41, 7635.
37. Tretinnikov, O. N.; Fujita, S.; Ogata, S.; Ikada, Y. J Polym Sci Part B: Polym Phys 1999, 37, 1503.
38. Tranchida, D.; Piccarolo, S.; Loss, J.; Alexeev, A. Macromolecules 2007, 40, 1259.
39. Maher, S. A.; Furman, B. D.; Babalola, O. M.; Cottrell, J. M.; Wright, T. M. J Orthop Res 2007, 25, 849.
40. Galeski, A. Prog Polym Sci 2003, 28, 1643.
41. Goldman, M.; Gronsky, R.; Ranganathan, R.; Pruitt, L. Polymer 1996, 37, 2909.
42. Lee, S. M.; Choi, S. W.; Nho, Y. C.; Song, H. H. J Polym Sci Part B: Polym Phys 2005, 43, 3019.